Willow: Practical WiFi Backscatter Localization with Parallel Tags

Jinyan Jiang[†], Jiliang Wang[†✉], Yijie Chen[†], Shuai Tong[†], Pengjin Xie[‡], Yihao Liu[†], Yunhao Liu[†]
[†]Tsinghua University, [‡]Beijing University of Posts and Telecommunications, Beijing, P.R.China
{jiangjy23, cyj20, tl19, liu-yh23}@mails.tsinghua.edu.cn,
{jiliangwang, yunhao}@tsinghua.edu.cn, xiepengjin@bupt.edu.cn

ABSTRACT

WiFi backscatter localization is a promising technology for the Internet of Things. However, existing works cannot work well for large-scale and low-cost tags with commodity WiFi devices. We present Willow, which provides accurate localization for parallel backscatter tags with commodity WiFi devices. We design a packet-level orthogonal backscatter modulation method to generate multiple orthogonal backscatter signals and support in-band backscatter with ambient WiFi. We show that backscatter signals can be effectively extracted even under strong in-band interference. To work in real WiFi traffic, we propose adaptive packet selection-based modulation to guarantee the orthogonality of backscatter signals. For parallel localization, we propose an iterative inter-tag interference cancellation method and a location filtering method to remove location ambiguity. We theoretically analyze the effectiveness of our method in supporting parallel tags. We prototype Willow tags using low-cost hardware and implement Willow AP on commodity WiFi NIC AX200. Through extensive experiments, we show that Willow achieves a median localization error of 27 cm and supports 51 parallel tags, which is 2× and 17× better than the state-of-the-art method.

CCS CONCEPTS

• **Networks** → **Cyber-physical networks**; • **Mobile information processing systems**; • **Global positioning systems**;

KEYWORDS

Backscatter, Wireless LocalizatiWiFion,

ACM Reference Format:
Jinyan Jiang, Jiliang Wang, Yijie Chen, Shuai Tong, Pengjin Xie, Yihao Liu and Yunhao Liu. 2024. Willow: Practical WiFi Backscatter Localization with Parallel Tags. In *The 22nd Annual International Conference on Mobile Systems, Applications and Services (MOBISYS '24), June 3–7, 2024, Minato-ku, Tokyo, Japan.* ACM, New York, NY, USA, 13 pages. https://doi.org/10.1145/3643832.3661853

1 INTRODUCTION

Backscatter communication enables low-power, low-cost, and ubiquitous connectivity to the Internet of Things (IoT), such as smart buildings, smart agriculture, and smart healthcare [1–11]. Many IoT applications need to know the location information of backscatter tags, which has encouraged advanced research in backscatter localization [12–21]. Given the widespread of WiFi, WiFi backscatter localization is considered a promising technology as it utilizes ubiquitous WiFi devices to achieve localization for backscatter tags. Moreover, with the continuous expansion of WiFi bandwidth and the increment of MIMO scale, backscatter localization based on WiFi signals can achieve increasingly higher accuracy.

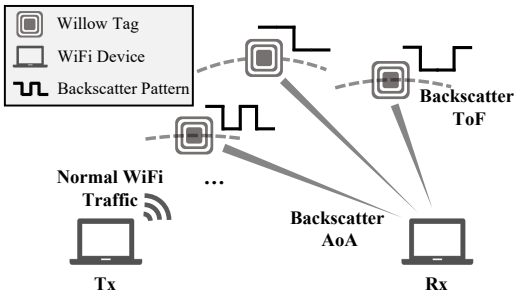

Figure 1: Willow provides parallel WiFi backscatter localization for low-cost tags with commodity devices.

There emerges an extensive collection of WiFi backscatter localization techniques, with representative ones shown in Table 1. Existing works, however, have the following limitations: **1) Spectrum efficiency.** To avoid in-band interference with excitation signals, previous backscatter systems shift the frequency of the excitation signal and make the backscatter signal out-of-band. For example, WiTag [6] shifts the backscatter signal into a non-overlapped band. However, considering tens, even hundreds of Mhz signal bandwidth in WiFi, frequency-shifting will lead to low wireless spectrum efficiency and high tag power consumption. Batch localization [8] utilizes OFDM modulation to obtain concurrent tag signals. However, maintaining orthogonality in OFDM requires a high-precision oscillator to control the shifting frequency and is difficult to achieve on low-cost tags. **2) Strong excitation interference.** Some works try to do in-band backscatter localization. TagFi [7] toggles backscatter tags and creates a new signal subspace based on the MUSIC spatial spectrum calculation, which partially separates backscatter signals from the excitation. However, the strength of the excitation signal is typically magnitudes higher than the backscatter signal, leading to inevitable residual interference with backscatter signals. **3) No parallel localization.** WiTag [6] and TagFi [7] only work for a single or very few tags. Batch Localization [8] supports parallel localization for multiple tags but is not compatible with commodity WiFi. In summary, none of the existing works achieves large-scale parallel localization with low-cost hardware platforms.

✉ Jiliang Wang is the corresponding author.

MOBISYS '24, June 3–7, 2024, Minato-ku, Tokyo, Japan

ACM ISBN 979-8-4007-0581-6/24/06
https://doi.org/10.1145/3643832.3661853

Table 1: Comparison with existing WiFi backscatter localization systems.

	Low-power tag	Parallel localization	Low excitation interference	Compatible with COTS WiFi	Spectrum consumption
WiTag [6]	✗	✗	✓	✓	High
Batch Loc. [8]	✗	✓	✓	✗	Medium
TagFi [7]	✓	< 4 Tags[1]	✗	✓	Low
Willow	✓	**✓(> 50 Tags)**	✓	✓	**Low**

[1] The localization error significantly increases according to their evaluation.

This paper presents Willow, the first **WiFi** **l**ocalization system for large-scale parallel **low**-power backscatter tags. As shown in Fig. 1, Willow takes packets from commodity WiFi devices as excitation signals. Instead of shifting signals out-of-band, a Willow tag only toggles between two reflection coefficients according to a certain pattern. The toggling rate is low to ensure low power consumption and low complexity for tags. We design orthogonal patterns for the reflection coefficients so that multiple backscatter signals along with the excitation signal can be simultaneously received and separated by commodity WiFi devices. The WiFi receiver analyzes the CSI (Channel State Information) in the received packets, separates the channel states of each tag, and calculates the locations of tags.

To turn the basic idea of Willow into reality, we need to address the following key challenges:

First, how to extract backscatter signals under strong in-band interference of excitation signals? Typically, we can generate backscatter signals by shifting the excitation signal out-of-band. This method works well for low-bandwidth excitation signals (*e.g.,* LoRa, Bluetooth, etc), but leads to high spectrum consumption and tag complexity for high-bandwidth signals like modern WiFi. The time division method cannot work here either. Because the backscatter signal is always derived from the excitation signal, it's impossible to assign different time slots to them. We propose a packet-level orthogonal backscatter modulation (POBM) method to embed backscatter signals into ambient WiFi traffic. We take a sequence of WiFi packets as excitation signals, where all packets have the same channel H. Willow tag reflects WiFi signals with different coefficients, e.g., -1 and 1. By carefully designing the coefficient pattern, we can construct a sequence that is orthogonal with the excitation signal and thus extract backscatter channels from excitation signals. For example, assume the backscatter channel is h and the coefficient pattern is $CP_B = [1, -1, 1, -1]$, the received CSI sequence will be $\hat{\mathbb{H}}(m) = [H, H, H, H] + CP_B \cdot h = [H + h, H - h, H + h, H - h]$, given each backscatter coefficient aligned with one WiFi packet. We derive the backscatter channel as $CP_B \cdot \hat{\mathbb{H}}(m) = 4 \cdot h$. The tag switches its coefficient pattern at the packet level, which can be easily achieved by low-power and low-complexity hardware.

Second, how to adapt to real WiFi traffic and devices? To extract the backscatter channel information, Willow requires orthogonality among coefficient patterns. Packets in real WiFi traffic may not accurately align with patterns in POBM. For example, there may be no packets for modulation in some periods. This destroys the orthogonality and leads to strong leakage from the excitation signal. We find that the coefficient pattern of the excitation signal is always 1, the backscatter tag only needs to create a pattern having an equal number of coefficients 1 and -1 to maintain the orthogonality. We design a packet selection mechanism to actively select the desired excitation packets, ensuring orthogonality between the backscatter signal and the excitation WiFi signal. Meanwhile, practical WiFi transceivers are not synchronized in time and frequency. It will create packet detection delay and overall phase offset, both leading to phase discontinuity among packets and destroying the pattern orthogonality. To settle this, we search for the best linear fit of the packet detection delay and phase offsets and then compensate them among different packets to achieve continuous phases.

Third, how to enable parallel backscatter localization? Some active localization systems such as GPS [22] listen to downlink traffic to enable concurrent localization. However, it requires the power-hungry down-conversion on the tag. In the context of WiFi backscatter localization, as the number of tags (uplinks) increases, the interference among tags significantly increases and thus degrades the localization accuracy. We design orthogonal POBM patterns for different tags, which can separate backscatter channels for each parallel tag. Then, we use the estimated backscatter channels for tag localization. To guarantee the orthogonality among backscatter signals, tags need to be time-synchronized when toggling. However, due to the restriction of power consumption and hardware complexity, some tags do not have synchronization circuits, which will break the orthogonality of parallel coefficient patterns. We introduce a two-level channel separation scheme to achieve parallel localization for unsynchronized tags. At the coarse level, we design a pseudo-orthogonal POBM pattern such that different tags can be semi-orthogonal. Further, at the fine-grained level, we propose an iterative interference cancellation method that searches and eliminates the strongest signal from the parallel transmissions, as the strongest one is the least influenced. We also find that tags with different signal powers are typically not co-located, due to the occurrence of similar multipath in nearby locations. We propose a location filtering algorithm to further decrease the interference. If a tag with a strong power is detected in one location, we can make sure that it will not be the location of the tag with a weak signal.

In summary, we have made the following contributions:

- We propose Willow, the first WiFi backscatter localization system for large-scale parallel low-power tags. We design a packet-level orthogonal backscatter modulation method to generate orthogonal in-band backscatter signals with ambient WiFi traffic. We analyze the requirements for maintaining the orthogonality between the tag and the excitation source and propose an active

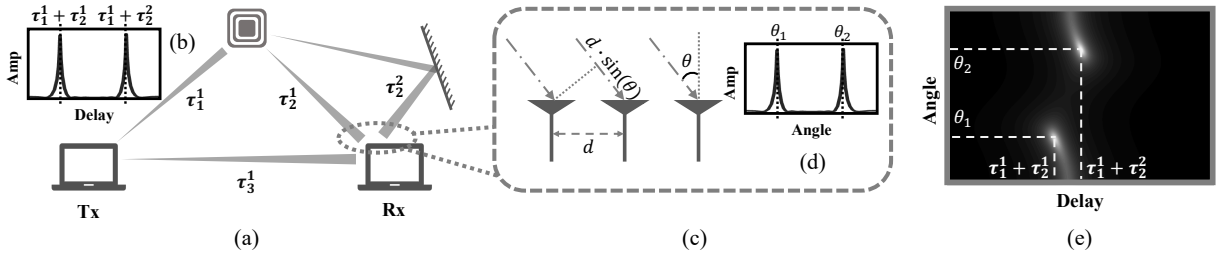

Figure 2: (a) Backscatter signal propagates along two paths to reach the Rx. (b) The MUSIC spectrum describes the signal propagation delay. (c) Incident angles create phase differences among antennae. (d) The MUSIC spectrum describes the incident angle. (e) The MUSIC spectrum describes both the time delay and incident angle.

selection method to adapt to real WiFi traffic. Finally, we propose an iterative cancellation and location filtering method to achieve parallel localization with the near-far problem.

- We prototype the Willow tag on a customized PCB board using commercial low-cost off-the-shelf circuit components. Willow can seamlessly work in the existing WiFi networks. We evaluate the performance of Willow extensively in different scenarios. The evaluation results show that Willow achieves a 27 cm median localization error and enables parallel localization for 51 tags. Compared with the state-of-the-art, Willow achieves 2× higher localization accuracy and 17× networking scale.

2 PRIMER

Signal propagation model. We first introduce the signal propagation model of WiFi backscatter. To emit the signal, a WiFi transmitter (Tx) first generates an OFDM signal in the baseband. We focus on the signal on one subcarrier as signals of other subcarriers go through a similar propagation process. Assuming the data transmitted is x, the baseband signal can be expressed as $s(t) = x \cdot e^{j2\pi f_p t}$, where f_p is the subcarrier frequency. Then, the Tx upper-converts the baseband signal with a high-frequency carrier as:

$$S(t) = s(t) \cdot e^{j2\pi f_c t} = x \cdot e^{j2\pi(f_p+f_c)t} \tag{1}$$

We first consider the LoS (Line-of-Sight) path of the backscatter signal. As shown in Fig. 2(a), the WiFi signal arrives at the backscatter tag with the attenuation α_1^1 and delay τ_1^1. The tag can switch between different states to modify the incoming signal and multiply it with different coefficients, denoted as y. Thus, the backscatter signal is:

$$S_B(t) = y \cdot \alpha_1^1 S(t - \tau_1^1) \tag{2}$$

Similarly, the backscatter signal propagates to a WiFi receiver (Rx) with another attenuation α_2^1 and delay τ_2^1. Thus, the backscatter signal received at the Rx is:

$$R_B(t) = y \cdot \alpha_1^1 \alpha_2^1 S(t - \tau_1^1 - \tau_2^1) = y \cdot x \cdot \alpha_1^1 \alpha_2^1 e^{j2\pi(f_p+f_c)(t-\tau_1^1-\tau_2^1)} \tag{3}$$

Here we ignore the time, frequency and phase misalignments between the Tx and Rx as they can be eliminated in the location calculation. The Rx down-converts $R_B(t)$ to the baseband by multiplying it with $e^{-j2\pi f_c t}$ as:

$$\begin{aligned} r_B(t) =& R_B(t) \cdot e^{-j2\pi f_c t} \\ =& y \cdot x \cdot \alpha_1^1 \alpha_2^1 e^{j2\pi(f_p+f_c)(t-\tau_1^1-\tau_2^1)} \cdot e^{-j2\pi f_c t} \\ =& y \cdot x \cdot \alpha_1^1 \alpha_2^1 e^{-j2\pi(f_p+f_c)(\tau_1^1+\tau_2^1)} \cdot e^{j2\pi f_p t} \end{aligned} \tag{4}$$

Then, the Rx applies FFT to $r_B(t)$ and checks the p^{th} point to get the channel of the backscatter signal:

$$\begin{aligned} \hat{h}_p = FFT_p\{r_B(t)\} &= y \cdot x \cdot \alpha_1^1 \alpha_2^1 e^{-j2\pi(f_p+f_c)(\tau_1^1+\tau_2^1)} \\ &= y \cdot x \cdot h_p \end{aligned} \tag{5}$$

where $h_p = \alpha_1^1 \alpha_2^1 e^{-j2\pi(f_p+f_c)(\tau_1^1+\tau_2^1)}$ is the channel of the backscatter signal. When there are multiple signal propagation paths, the estimated channel will be a linear superposition of multipath signals. For example, there are two propagation paths in Fig. 2(a). The backscatter channel will be: $h_p = \alpha_1^1 \alpha_2^1 e^{-j2\pi(f_p+f_c)(\tau_1^1+\tau_2^1)} + \alpha_1^1 \alpha_2^2 e^{-j2\pi(f_p+f_c)(\tau_1^1+\tau_2^2)}$. Here we neglect the reflected signals (including the signal scattered by other tags) scatter again as previous works [2, 23, 24] do. Because they are too weak to capture in the MUSIC spectrum.

Localization model. After extracting the backscatter channel h_p, we can locate the tag. The Rx can measure the wireless channel at different subcarriers and apply the MUSIC algorithm [25] to the channel to obtain the CIR (Channel Impulse Response). CIR describes the propagation delay of each signal path and can reflect the distance between tags and Tx/Rx. When there are multiple signal paths, the MUSIC spectrum will exhibit them all, for example, $\tau_1^1 + \tau_2^1$ and $\tau_1^1 + \tau_2^2$ in Fig. 2(b). Rx can also obtain AoA (Angle of Arrival) information that measures the channel by the multiple antennae. The phase (propagation distance) differences between adjacent antennae are proportional to $sin(\theta)$, where θ is the AoA of this path. As shown in Fig 2 (c) and (d), the incident phase is shown as distinct peaks in the MUSIC spectrum [26]. Rx can use the channel from both multiple subcarriers and antennae to joint-estimate the ToF and AoA simultaneously [27, 28]. After Rx obtains channel measurements in subcarrier #p and antenna #q, $h_{p,q}$, it performs eigenvalue decomposition to the CSI matrix and calculates the energy intensity for each ToF-AoA combination with 2D-MUSIC algorithm [29]. For example, in Fig. 2(a), there are 2 multipath, and the corresponding MUSIC spectrum will create two

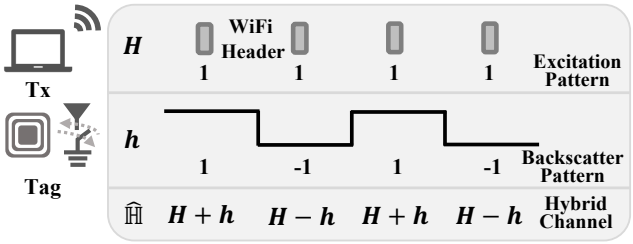

Figure 3: Tag toggles between two coefficients to enable packet-level orthogonal backscatter modulation.

separated spots lying in the pair of $\{\tau_1^1 + \tau_2^1, \theta_1\}$ and $\{\tau_1^1 + \tau_2^2, \theta_2\}$, as shown in Fig. 2(e). We ignore the time misalignment between Tx and Rx, as it can be calibrated by the distance and measured delay between them. We only need to get the {ToF, AoA} pair with the shortest time delay to identify the LoS path. With the LoS ToF, we know the sum of the Tx-to-Tag and Tag-to-Rx distance. We can then determine an ellipse based on the location of the Tx and Rx. With the aid of LoS AoA, we can determine a ray starting from the Rx. The intersection of the ellipse and ray is the tag location. Willow can also use more Rx to find their intersection to provide higher accuracy.

2.1 Challenges

The Backscatter channel is mixed with strong in-band excitation interference. We assume that we could extract pure backscatter channel h. However, since Willow tags work in the same frequency band with the excitation signal, the channel estimated by Rx will be mixed with the excitation channel. Similar to Eq. 5, the excitation channel is $\hat{H}_p = x \cdot H_p$. In Fig 2(a), the channel of excitation signal is $H_p = \alpha_3^1 e^{j2\pi(f_p+f_c)\tau_3^1}$. The hybrid channel can be expressed as:

$$\hat{\mathbb{H}}_p = \hat{H}_p + \hat{h}_p = x \cdot H_p + y \cdot x \cdot h_p \tag{6}$$

It is challenging to extract the backscatter channel from Eq. 6.

Compatible with real WiFi traffic and devices. Willow tag creates an orthogonality pattern to extract the backscatter channel and try to avoid interference from the excitation signal. However, real WiFi traffic is not always uniform and desynchronization between transceivers will lead to the destruction of orthogonality and leaked interference from the excitation signal. Considering the greatly stronger power difference between backscatter and excitation signal, which can be up to tens of dB [24], the residual error of excitation will dramatically distort the estimation of the backscatter channel and thus disable the localization.

Inter tag interference in parallel localization. In parallel localization, there are more terms in Eq. 6 to be resolved. Willow assigns different orthogonality patterns to different tags. However, the time misalignments among tags also destroy the orthogonality. To make matters worse, the tag with a stronger signal strength may leak its channel value to the weaker ones, known as the near-far problem. In lower-cost tags, this near-far problem is more difficult to deal with due to the lack of a synchronization mechanism. Willow should ensure the robustness of the system in this case.

3 WILLOW BASIC DESIGN

We first introduce how Willow works for a single tag and then extend it to parallel localization in the next section.

3.1 Extract Backscatter Channel

To extract the backscatter channel h, we need to separate it and the excitation channel H from the hybrid channel measurement $\hat{\mathbb{H}}$. We use the POBM scheme to achieve this.

We first see how a standard WiFi receiver estimates the wireless channel. WiFi transmitters send packets sharing the same preamble to enable channel measurement and calibration, known as LTF (Long Training Field). In other words, the transmitted data x of LTF in Eq. 6 remains unchanged for different packets. In the WiFi standard, the LTF is pre-defined for every subcarrier. Without loss of generality, we assume the coefficient in every WiFi packet is set to 1, i.e., x is consistently equal to 1. In fact, x is either 1 or -1 for different subcarriers in WiFi. But both cases can be normalized to 1, which doesn't affect the orthogonality in POBM. Therefore, for the m^{th} packet, the receiver estimates the channel based on the LTF as $\hat{H}(m) = x(m) \cdot H = H$. Then, we discuss how the backscatter signal impacts the channel estimation. Backscatter tags can toggle between two states, which introduces two different coefficient values for each arrived WiFi packet. For the m^{th} incident packet, the tag multiplies it by $y(m) = \{-1, 1\}$ as shown in Eq. 2. Note that even if the coefficients are not -1 and 1, we can always regard them as -1 and 1 with a DC offset and linear scaling, without affecting the orthogonality in POBM either. After superposing a backscatter signal, the channel for the m^{th} packet can be expressed as $\hat{h}(m) = y(m) \cdot x(m) \cdot h = \pm h$.

Signals in an actual WiFi channel contain both the excitation and backscatter signals. Thus, the measured hybrid channel is $\hat{\mathbb{H}}(m) = H \pm h$. Our goal is to separate backscatter channel h from the actual estimated channel $\hat{\mathbb{H}}(m)$. As shown in Fig. 3, the coefficients in LTF compose a coefficient pattern $CP_E = [1, 1, 1, 1]$. Meanwhile, the tag toggles the coefficient for different packets to generate an orthogonal coefficient pattern, *e.g.*, $CP_B = [1, -1, 1, -1]$. The hybrid signal is the combination of these two patterns. For each packet, the Rx estimates the hybrid channel and outputs a sequence: $\hat{\mathbb{H}} = CP_E \cdot H + CP_B \cdot h = [H + h, H - h, H + h, H - h]$. To extract backscatter channel h from the estimated $\hat{\mathbb{H}}$ sequence, Willow dot multiplies $\hat{\mathbb{H}}$ with the predefined backscatter coefficient pattern, i.e., $\hat{\mathbb{H}} \cdot CP_B = (H + h) - (H - h) + (H + h) - (H - h) = 4 \cdot h$. By normalizing the result, Willow gets the pure backscatter channel: $\frac{4 \cdot h}{4} = h$. Similarly, by multiplying the received channel sequence with the pattern corresponding to the excitation source CP_E, Willow can get the pure excitation channel H.

With the POBM method, Willow can also capture the weak backscatter channel. Due to the strong excitation interference, when the tag toggles between two coefficients, it only creates little influence for the hybrid channel shown in Fig. 4(a). However, with the POBM and according decoding method, we get the pure backscatter channel estimation as shown in Fig. 4(b). Since the Willow tag only needs to toggle from different coefficients in a packet level, regardless of the original bandwidth of the excitation signal, it ensures low power consumption and hardware complexity on the tag. A designed pattern here can also resist the dynamic environment.

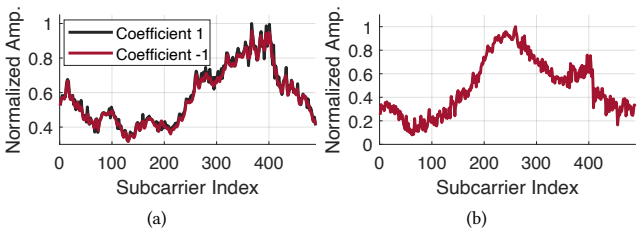

Figure 4: (a) CSI amplitude of hybrid channel with backscatter coefficient 1 and -1 (b) CSI amplitude of extracted backscatter channel.

Assuming there are walking people, it will also affect the hybrid channel with certain patterns. The typical frequency of a human walking is around 1.8 to 2 Hz [30]. Willow chooses a different toggling frequency from 20 to 100 Hz to avoid this interference [7].

3.2 Time Misalignment

The POBM method needs orthogonality between patterns, which requires the excitation source and tag to transmit synchronically. Willow could achieve this by setting the toggling rate of the tag the same as the excitation packet sending rate. Ideally, even if the tag is not synchronized with the excitation source, as long as the period of them is the same, the Rx is still able to collect all the necessary coefficients. As shown in Fig. 5(a), the tag starts sending coefficients with a certain time offset t_1. If the tag can hold the current state for exactly the same time interval, the next packet will be with the targeted next backscatter coefficient. The Willow tag can blindly toggle its switch without a synchronization circuit.

However, as WiFi adopts the CSMA/CA mechanism where a transmitter first detects the ongoing traffic and delays its next transmission accordingly, the interval between two adjacent WiFi packets may vary. If the delay is too large, the tag may switch to the next coefficient. As shown in Fig. 5(b), the packet #2 is delayed by Δt. If Δt is larger than the scheduled packet interval t_1, then the second coefficient sent by tag is not -1, but 1. Correspondingly, the second channel measurement $\hat{\mathbb{H}}(2)$ is no longer the targeted one $H - h$, but is $H + h$. The coefficient pattern of the tag now is $[1, 1, 1, -1]$, which is not orthogonal to CP_E anymore.

We qualify the distribution of delay in a practical wireless environment with an experiment. We use a commodity WiFi NIC AX200 to send packets every 20 ms in a laboratory. We analyze the time intervals between adjacent packets by checking the timestamp of received packets. The result shows that the maximum interval is around 22 ms, which means the extra delay can be up to 2 ms.

However, we have a key observation here: the pattern of the excitation signal is only composed of coefficient 1, *i.e.*, $CP_E = [1, 1, ..., 1]$. Thus, for a backscatter pattern $CP_B = [C_1, ..., C_j = \pm 1, ...]$, the dot multiplying with CP_E is the sum of every coefficient, which is equal to the number of coefficient 1 minus the number of coefficient -1:

$$\begin{aligned} CP_B \cdot CP_E &= [1, 1, ...] \cdot [C_1, ...C_j = \pm 1, ...] \\ &= C_1 + ... + C_j = \pm 1 + ... \\ &= num(C = 1) - num(C = -1) \end{aligned} \tag{7}$$

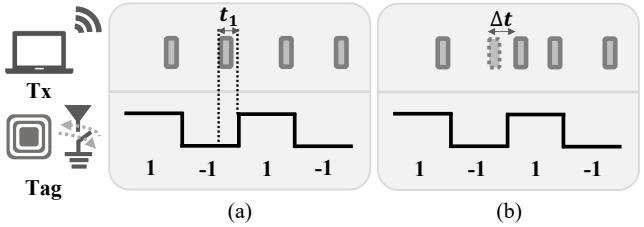

Figure 5: (a) Ideal case when Tx is transmitting packets uniformly. (b) There is a jitter for the second packet.

Thus, if the pattern is composed of the same amount of coefficients 1 and -1, the result of Eq. 7 is 0, *i.e.*, CP_B is still orthogonal with CP_E. The Rx can process the timestamp of each packet, through which it can calculate the packet intervals and infer the coefficient value of each packet. Then, it can calculate the difference between the number of coefficient 1 and -1. In the example of Fig. 5(b), the Rx will know the received backscatter pattern is $[1, 1, 1, -1]$. This pattern has two more coefficients 1. Willow only needs to select the same number of coefficient 1 to meet the number of -1 now. In this case, Willow can pick any one of coefficient 1 from the first three packets and the coefficient -1 from the last packet.

As the unexpected delay is randomly distributed, both coefficients 1 and -1 have the same possibility of being transferred. The mathematical expectation number of coefficients 1 and -1 should be equal. We further consider the expectation of the minimum number of 1 and -1 (*i.e.*, $\mathbb{E}[\min(num(1), num(-1))]$). Suppose we have a pattern containing $2M$ coefficients, and the possibility of flipping is a, then the number of 1 or -1 follows the binomial distribution $B(M, 2Ma(1-a))$. According to the central limit theorem [31], this distribution can be approximated to the normal distribution $N(M, 2Ma(1-a))$. The probability density function of the number of 1 or -1 as $p(x) = \frac{1}{\sqrt{4\pi Ma(1-a)}} e^{-\frac{(z-M)^2}{4Ma(1-a)}}$. By exploiting the symmetry of 1 and -1, we calculate the expectation $\mathbb{E}[\min(x_1, x_2)] = 2\int_0^M xp(x)\mathrm{d}x$. If the coefficient number $2M$ is 100, even in the worst case that coefficients flip fully randomly ($a = 0.5$), we have this expectation to be 46. This means that more than 90% ($46 \times 2/100$) coefficients can be selected to ensure an equal number of 1 and -1. This also indicates that even for aperiodic packets, such as burst data packets with fully non-uniformed time intervals, its impact on Willow can still be eliminated by carefully selecting orthogonal coefficient patterns with low overhead.

3.3 Unsynchronized Transceivers

The excitation source generates the same packet header on the baseband. Willow utilizes it and creates a coefficient pattern full of coefficient 1. However, there are PDD (Packet Detection Delay) and CFO (Carrier Frequency Offset) among unsynchronized commodity WiFi devices [25, 28]. The PDD δ will add an extra linear phase $2\pi f_p \delta$ into different subcarriers in a packet. The CFO will cause an overall phase offset β when the transceivers up/down-converting the baseband signals. Thus, the m^{th} actual hybrid channel measurement in subcarrier #p and antenna #q of the Rx is:

$$\hat{\mathbb{H}}'_{p,q}(m) = \hat{\mathbb{H}}_{p,q}(m) \cdot e^{-j2\pi f_p \delta_m} \cdot e^{j\beta_m} \tag{8}$$

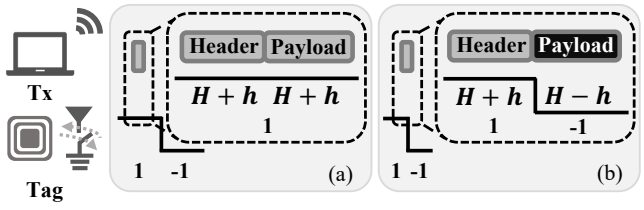

Figure 6: (a) Tag doesn't toggle during the transmission. (b) Tag toggles during the transmission.

These two types of offset are consistent for different antennae in the same packet because the different receiving chains are synchronized. But they vary among packets, which makes the pattern of the excitation signal no longer all consist of coefficient 1 and ruins the orthogonality. To tackle this problem, Willow applies the widely used CSI sanitization algorithm in MonoLoco [27], TagFi [7], and SpotFi [28]. Willow first calculates the unwrapped phase value $\Phi_{p,q}(m)$ of CSI measurement $\hat{\mathbb{H}}'_{p,q}(m)$. Then, Willow finds the best linear fit and overall offset value to cancel the residual offset in the unwrap phase:

$$[\hat{\delta}_m, \hat{\beta}_m] = \arg\min_{\rho,\xi} \sum_{p,q=1}^{P,Q} \left(\Phi_{p,q}(m) - 2\pi f_p \rho - \xi\right)^2 \tag{9}$$

Then, Willow compensates the phase value in the measured channel $\hat{\mathbb{H}}'_{p,q}(m)$ by the estimated $\hat{\delta}_m$ and $\hat{\beta}_m$, which gives us: $\hat{\mathbb{H}}'_{p,q}(m) \cdot e^{-j2\pi f_p \hat{\delta}_m} \cdot e^{-j\hat{\beta}_m}$. This process eliminates the phase offset caused by unsynchronized transceivers. The excitation source is still sending the pattern full of coefficient 1 and is ready for Willow to extract the backscatter channel.

3.4 Working with existing WiFi

Willow tag does not require a special packet format from the excitation source and can tolerate time misalignment to the excitation. Thus, Willow is completable with commodity WiFi transmitters. For commodity WiFi receivers, they will apply standard channel estimation as described in Eq. 6. The tag path is regarded as a normal multipath, which can be seamlessly captured by the WiFi hardware. Thus, Willow is also completable with commodity WiFi receivers.

But for an unsynchronized Willow tag, there are two possible situations for ongoing WiFi transmission. First, if the tag doesn't toggle state during the packet, as shown in Fig. 6(a). The commodity WiFi Rx will process the header and get the channel estimation $\hat{\mathbb{H}}(1) = H + h$. For the payload, the baseband signal x_{data} will also go through the same channel. Thus, the received data will be $\hat{\mathbb{H}}(1) \cdot x_{data}$. By dividing the received data with the channel estimated by the header, Rx recovers the original data: $\hat{\mathbb{H}}(1) \cdot x_{data} / \hat{\mathbb{H}}(1) = x_{data}$. This process is done seamlessly by the commodity receiver. So, it won't affect the excitation transmission. We note that because of the short packet duration for active WiFi packets, the possibility of this case is large. For example, if the duration of each coefficient state for the backscatter signal is 10 ms, and the duration of WiFi packets is 60 μs, the possibility for the second case is only $1 - 2 \cdot \frac{60\ \mu s}{10\ ms} = 98.8\%$. The second situation is tag toggles its coefficient during the ongoing packet, as shown in Fig. 6(b). Here we assume a representative case in which the tag toggles its coefficient after the header. The estimated channel is $\hat{\mathbb{H}}(1) = H + h$. But the undergo channel for payload data is $\hat{\mathbb{H}}(2) = H - h$. If the Rx tries to recover payload data by $\hat{\mathbb{H}}(2) \cdot x_{data} / \hat{\mathbb{H}}(1)$, there will be extra noise h in decoding. We take advantage of the POBM method to avoid the impact of backscatter signals on the decoding of normal WiFi packets. As POBM can tolerate extremely low SNR backscatter signals, the backscatter channel h can be regarded as a negligible noise term in decoding a single packet. In a typical WiFi backscatter network, the power difference between the source and tag is normally up to 40 dB [32]. For example, a WiFi packet with 20 dB SNR, an interference source that is 40 dB weaker, only increases the BER by 2.6^{-5} with 256 QAM modulation [33]. For packets with 64-byte payload, the PRR is only degraded by 0.16% [34]. Considering the possibility of this case, the overall PRR loss $0.16\% \times (1 - 98.8)\% = 1.92 \times 10^{-5}$, which is negligible.

4 PARALLEL LOCALIZATION

When there are multiple tags, Willow uses the POBM to separate channels of parallel tags and locate multiple tags simultaneously. To achieve this, Willow assigns different orthogonal coefficient patterns to different tags. Each tag toggles its states according to the predefined coefficient pattern. Then, the WiFi Rx collects the channel which contains an excitation and multiple backscatter channels. With the carefully designed interference separation approach, Willow Rx can get the pure channel for each backscatter tag. Finally, Willow calculates the location for each tag based on the localization model mentioned in § 2.

4.1 Synchronized Tags

We first focus on the case with synchronized tags, where tags and the excitation source are time-synchronized. Thus, they can generate the arranged coefficients in the same time slot, as shown in Figure 7(a). In this case, we assign fully orthogonal patterns to different tags to cancel inter-tag interference. Considering the possible jitter from the sending time of excitation packets, we extend the coefficient duration at tags, promising each packet falls into one coefficient slot. Willow can achieve the synchronization by a leader-follower mechanism [32, 35]. The excitation source wakes the tag by a certain interval, tags will use a simple envelop detector to recognize the interval and set the common starting time of patterns sending.

For example, there are two synchronized tags, as shown in Fig. 7(a). Willow assigns two orthogonal patterns: $CP_B^1 = [1, 1, -1, -1]$ and $CP_B^2 = [1, -1, 1, -1]$. Those two tags toggle coefficients accordingly and simultaneously. The hybrid channel $\hat{\mathbb{H}}(m)$ now contains both excitation channel H and two backscatter channels h^1 and h^2: $\hat{\mathbb{H}}(m) = [H + h^1 + h^2, H + h^1 - h^2, H - h^1 + h^2, H - h^1 - h^2]$ If we dot multiply the received channel $\hat{\mathbb{H}}(m)$ with CP_B^1, we will get the channel measurements of h^1. Similarly, we get h^2 by dot multiplying the channel sequence with CP_B^2. Willow adopts the widely used Walsh code to generate the assigned patterns. In Walsh code, it always contains the excitation pattern CP_E which only consists of coefficient 1. Willow tags choose other patterns different from CP_E to keep the orthogonality.

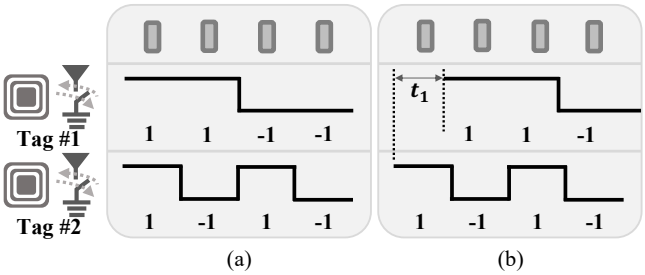

Figure 7: (a) Synchronized tags toggle simultaneously. (b) Unsynchronized tags have a time offset.

4.2 Unsynchronized Tags

Then, we look at the situation with unsynchronized tags. The lack of time synchronization will break the orthogonality between the assigned coefficient patterns. As shown in Fig. 7(b), the pattern for tag#1 now is $CP_B^1 = [0, 1, 1, -1]$, which is not orthogonal with $CP_B^2 = [1, -1, 1, -1]$. The time asynchronization also exacerbates the near-far problem. It makes the signal from tags with stronger power strength leak to the weaker ones. A straightforward idea for the near-far problem is to use a central AP to explicitly lower the power of stronger tags [23]. However, unsynchronized tags cannot receive down-link arrangements. We propose several designs to ease the tag asynchronization-induced interference problem. First, Willow uses the S-Kasami sequences to generate the pattern, which is a "pseudo-noise" sequence and can lower the correlation between unsynchronized patterns. Then, Willow adopts an interactive elimination method to further decrease the leaked signal. At last, Willow adopts a location filtering method to filter out the unwanted locations caused by the residual leaked signal.

4.2.1 Iterative Elimination. We have a key observation here: the signal of the strongest strength is typically least influenced by other signals. Willow can calculate the channel of the tag with the current strongest strength, and then cancel it in the hybrid signal and proceed to the next round. This idea is widely used in multi-signal separation [36, 37]. In Willow, however, we have a different restriction. In backscatter systems, due to more signal propagation attenuation, the power of the excitation signal is typically several orders of magnitude stronger than the backscatter signal [24, 32, 38]. Thus, the strongest terminal is always the excitation source with the pattern consisting of all coefficients 1. Even a small residual error in the elimination process for the excitation source will spread into the estimation of the backscatter channel and greatly degrade the localization accuracy. Willow avoids this by always ensuring the orthogonality between the excitation signal and the backscatter signal. Here, Willow also adopts the active packet-picking method in § 3.2. Moreover, we extend the one coefficient duration according to the scale of the network to lower the possibility of the coefficient flipping caused by the jitter of excitation packets sending.

To be specific, after receiving a channel sequence containing multiple tag signals with arbitrary time offsets, Willow uses a sliding window and the predefined pattern to find the strongest backscatter signal. During this process, Willow also actively picks packets to form backscatter patterns with equally distributed coefficients 1 and -1 to avoid strong interference from the excitation source. After extracting the current strongest backscatter channel, Willow subtracts the channel value from the hybrid channel and encounters the next round of calculation, till the channels of every tag are obtained. The simulation results show our method can provide a dynamic range of up to 60 dB.

4.2.2 Location Filtering. After using the quasi-orthogonal pattern and iterative elimination, we lower the signal leakage among tags. However, there is always residual error which will be leaked among backscatter channel measurements. When applying dot multiplication of the channel sequence with the target pattern of a specific tag, the residual error from other tags will be added to current channel measurements. This phenomenon is essentially equal to adding more multipath which accords to the location of those tags with stronger signal strengths. When it acts on the MUSIC spatial spectrum, there will appear more pseudo peaks. Here we find a key fact that the tag with a significantly weaker power is more likely to be far away from those with a stronger power. To filter those pseudo peaks, Willow first records the location of stronger tags. When locating those weaker tags, there may appear an unwanted location corresponding to those stronger tags. Willow actively ignores the location that appeared before and picks the targeted location.

To be specific, Willow also follows the iterative style for location filtering. In each round, Willow always locates the current strongest tag. It first checks all the possible locations corresponding to the MUSIC spatial spectrum which exhibit hot dots. Then, it selects the location among all the possible locations with the highest weight. Initially, the weight w_k of location k is set to the value of $w_k = 1/d_k$, where d_k is the sum of Tx-to-k distance and k-to-Rx distance. The initial weight design implies that Willow tends to choose locations with a lower ToF value because the target LoS path is always the shortest. In each round of filtering, the selected target location will refresh the whole area weight. For a location with weight w, whose distance from the selected location is D, and the power of the current strongest tag is P, the updated weight $w' = w - P/D$. With this proposed location filtering method, Willow further decreases the inter-tag interference.

5 IMPLEMENTATION

Willow Tags. We develop two types of backscatter tags: synchronized and unsynchronized tags. Both use off-the-shelf components including an ADG902 [39] RF switch, a 2.4 GHz omnidirectional antenna with a gain of 5 dBi, and an STM32L011D3P6 [40] low-power microcontroller unit (MCU). The synchronized tags incorporate an additional downlink detection module, which employs an envelope detector. The envelop detector contains a voltage doubler rectifier circuit that can extract the envelope of the WiFi RF signal. It employs Schottky diodes SMS7630-005LF [41], and a voltage comparator LPV7215 [42]. This envelope is then compared at a voltage comparator with a pre-set threshold voltage. The comparator can output high or low levels to indicate the presence or absence of WiFi data packets. The tags achieve synchronization by recording and matching the time intervals between WiFi packets. Because Willow tag uses packet-level modulation The power consumption for tags is around 108 μW.

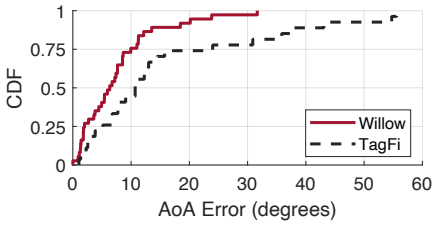

Figure 8: AoA error in the office.

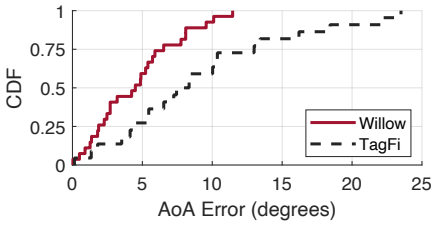

Figure 9: AoA error in the open field.

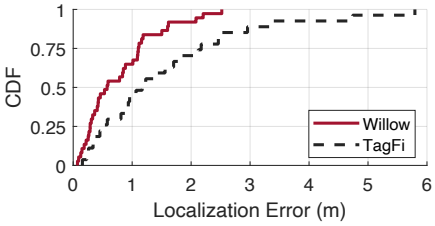

Figure 10: Localization error in the office.

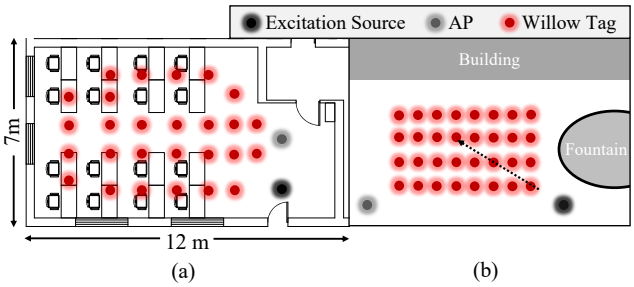

Figure 11: (a) Tag placement in the office. (b) Tag placement in the open field.

Excitation source and AP. The excitation source and AP are x86 PCs with Intel AX200 [43] WiFi NIC. We use the PicoScenes [44] to collect CSI measurements from 2 antennae and 489 subcarriers. The Wi-Fi NIC is configured to operate on 2422 MHz with a bandwidth of 40 MHz. All transceivers use 2.4 GHz omnidirectional antennae with a gain of 5 dBi. The POBM method requires the received training field of excitation signals to remain the same among packets. Although the baseband value of this field is predefined and fixed, we need to fix the transmitting power and the receiving gain. It's feasible for AX200 to fix the transmitting power, but we can't set the receiving gain. So, in our implementation, we filter out those packets with outlier magnitude. Other WiFi NICs which provide a specific gain value or fixed receiving gain can also be adopted here [45].

6 EVALUATION

6.1 Micro Benchmark

We evaluate the localization performance of Willow and compare it with a previous work TagFi [7], a state-of-the-art WiFi backscatter localization system with commodity WiFi transceivers. TagFi toggles the tag and creates a new subspace from the excitation signal in the same MUSIC spatial spectrum. We use the same hardware design and the same amount of AP when conducting comparisons with TagFi. The localization accuracy depends on many factors, such as the multipath environment, AP (Rx) density, SNR, etc. In this section, we test the performance of Willow with different factors. Tag toggles with a coefficient pattern of $[1, -1, ..., 1, -1]$ with a frequency of 100 Hz.

6.1.1 Angle estimation accuracy. We experiment in an indoor office to evaluate the angle estimation accuracy of Willow. We move one tag to different places and measure the angle estimation error in the AP. The placement of tags and AP are shown in Fig. 11(a). The tag is placed uniformly in this room, with some placement where there are obstacles such as furniture between the tag and Rx. At each place, according to the SNR of the backscatter signal, we use 50 to 200 pattern length to calculate the backscatter channel. We plot the CDF (Cumulative Distribution Function) of the angle estimation error, as shown in Fig. 8. Willow achieves a median angle estimation error of 6.3 degrees. However, TagFi suffers from strong in-band excitation signal interference, the median error is 10.7 degrees. We also observe that TagFi goes through a much more severe long-tail effect. The 90^{th} percentile tail error is 13.5 degrees for Willow compared to 38 degrees for TagFi. This is because the multipath relationship decides the amount of interference from the excitation source. The error can be significant in specific places. We will evaluate this phenomenon in § 6.1.4. We also evaluate the performance in an open field, in which the multipath is weaker, as shown in Fig. 11(b). As shown in Fig. 9, the median error of Willow and TagFi both decrease to 4.5 degrees and 7.4 degrees respectively. Willow outperforms TagFi in different scenarios.

6.1.2 Location estimation accuracy. Both Willow and TagFi can find the intersection of multiple locating results from multiple APs to infer the final location of the tag. In this experiment, we measure the location estimation error. We place another three to four APs on the random corner of experimental fields. Each AP picks the useful backscatter channel based on accordingly SNR. The average distance between different APs is around 9 m. The result for the indoor office is shown in Fig. 10, the median error of Willow is 57.5 cm. However, the median error of TagFi is 117 cm. The result for the outdoor field office is shown in Fig. 12. The median error of Willow and TagFi is 27 cm and 54.4 cm respectively.

6.1.3 Accuarcy under different AP densities. We put four or five APs in the indoor office to verify the impact of collaborative APs. In this experiment, we extend the pattern length to 250 to make sure every AP receives the backscatter signal with sufficient SNR. The result is shown in Fig. 13. More APs will average the noise and improve the accuracy. The median localization errors for Willow decrease to 52.6 cm and 32.7 cm for four and five APs respectively. For TagFi, the median localization errors are 116 cm and 66.5 cm. We notice that there is more improvement for TagFi than Willow. This is because, for TagFi, the geometrical relationship will greatly influence the localization results for the backscatter tag. When there are more APs, it will create various relative angles for the excitation source and the tag. However, even Willow with four APs still outperforms TagFi with five APs.

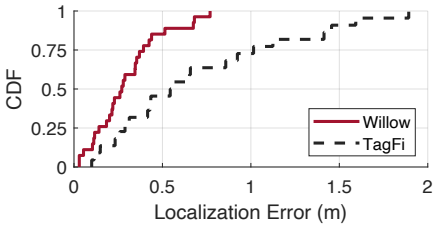

Figure 12: Localization error in the open field.

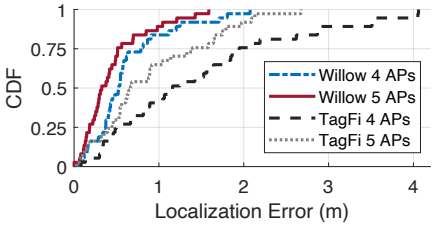

Figure 13: Localization error with different densities of AP in the office.

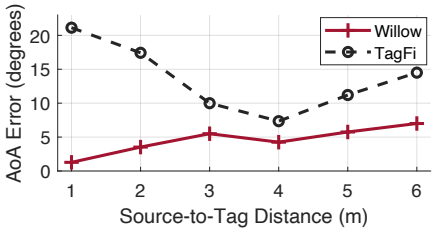

Figure 14: Localization error with different Source-to-Tag distance.

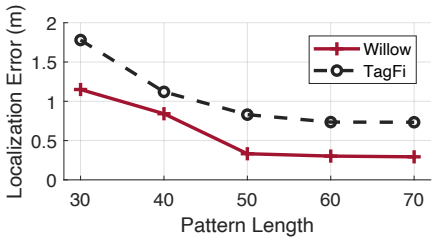

Figure 15: Localization error with different pattern lengths.

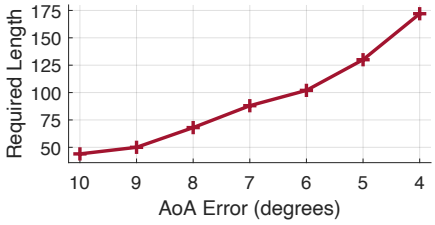

Figure 16: Minimal length to achieve specific accuracy.

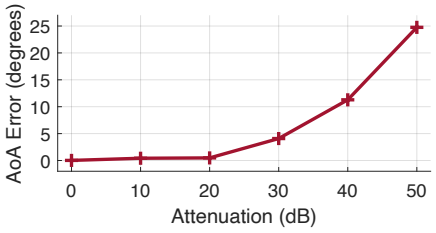

Figure 17: AoA error with different attenuation on LoS path.

6.1.4 Impact of the geometrical relationship between tag and AP. Willow extracts the pure backscatter channel by the orthogonal coefficient pattern with POBM. However, TagFi calculates the MUSIC spectrum for the backscatter signal with the presence of the excitation signal. If the tag is closer to the source, the inferred AoA and ToF for the tag and source are also closer. It means the peak of the excitation signal will cover the backscatter signal more easily. Thus, the geometrical relationship between tag and AP will influence the localization results of TagFi greatly. We experiment in the open field to evaluate this effect. We fix the distance between the excitation source and the AP and gradually move the tag away from the source along the dashed line in Fig. 11(b) to verify the impact of the geometrical relationship of devices. The distance between the tag and the source varies from 1 m to 6 m. As this distance increases, the interference from the source will decrease. We measure the angle estimation error at each location. The results are shown in Fig. 14. When the tag is close to the excitation source, TagFi exhibits a high angle estimation error of more than 20 degrees. That is because the strong interference from the excitation source masks and distorts nearby backscatter peaks in the MUSIC spectrum. However, the error for Willow in this case is only 1.3 degrees. As the distance increases, the error of Willow also approximately increases because of the decrement of SNR. But for TagFi, its error first falls abnormally and then increases. It shows that TagFi is greatly influenced by the geometrical relationship between tag and AP. However, Willow achieves lower error regardless of the relative location of the tag.

6.1.5 Impact of pattern length. The length of the backscatter pattern affects the SNR of the backscatter signal and the localization accuracy. We fix the distance between the tag and source to 2 m and change the length of the coefficient pattern from 30 to 70. We note that for higher localization accuracy or longer source-to-tag distance, Willow does need a longer pattern length to achieve the trade-off between system performance and localization latency. In this experiment, we measure the localization estimation error for each length of the coefficient pattern. The result is shown in Fig. 15. When the length is only 30 packets, the localization error is 115 cm for Willow. At the same time, the error for TagFi is however 178 cm. As the length increases, the localization error decreases gradually and finally reaches 29.3 cm when the length is 70 packets. Willow achieves lower localization error for any length of the pattern.

6.1.6 Pattern length for different accuracy requirements. To verify the required pattern length regarding the AoA estimation accuracy, we examine the minimal needed length to achieve different accuracies in the indoor office. We place the tag 5 meters away from the AP. We set the target accuracy from 10 degrees to 4 degrees, and then we make the tag consistently output the coefficient pattern and record the minimal packets needed to achieve the target accuracy. The result is shown in Fig. 16. As the accuracy requirement increases, Willow needs more packets to improve the accuracy. From 10 to 9 degrees, we only need 6 extra packets. But it needs 42 packets from 5 to 4 degrees. We only test the performance of Willow here because it can achieve an accuracy of less than 4 degrees in this experimental setting.

6.1.7 Impcat of obstacles. The obstacle between the excitation source and the tag will decrease the signal strength of the LoS path. Thus the spot of the multipath signal in the MUSIC spectrum will make it easier to cover the spot of the target LoS path and decrease the localization accuracy. After checking the indoor experiment results in § 6.1.1, those results with large errors (the long-tail) typically happen with the NLoS scenario. But even in this NLoS case, Willow can still identify the direct path with weaker signal strength by tracking the path in the 2-D MUSIC spectrum with the

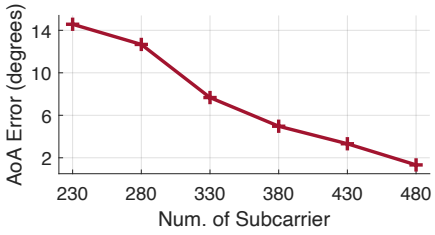

Figure 18: AoA error with different numbers of subcarriers.

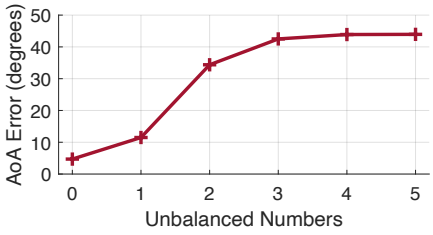

Figure 19: AoA error with different unbalanced numbers of coefficients.

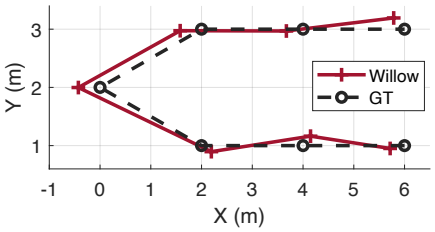

Figure 20: Tracking object trajectory.

shortest time delay like many previous papers do [2, 25, 28]. To verify its impact, we conduct a trace-based simulation experiment to verify the effect of obstacles on the localization accuracy. We assume there are two paths, one of them is LoS path and the other one is a reflection path with a propagation of 3 and 6 m respectively. Then we gradually add attenuation to the LoS path and check the AoA estimation error to verify the impact of different degrees of obstacles. The result is shown in Fig. 17. Willow can support accurate AoA results with 20 dB attenuation. Even with 30 dB attenuation, the error is slightly increased to 5 degrees.

6.1.8 Impact of bandwidth. The bandwidth affects the localization accuracy from the following two aspects. First, more subcarriers (bandwidth) provide more diversity gain and thus increase the SNR. Second, it also increases the ability to distinguish the multipath as it infers a finer-grained time delay profile. In this experiment, we set the distance between the excitation source and the tag to 5 meters in the indoor office. Then we gradually increase the number of used subcarriers from 230 to 480 and measure the AoA estimation accuracy. The result is shown in Fig. 18. The error drops from 14.6 degrees to less than 2 degrees when using 230 and 480 degrees.

6.1.9 Packet selection. To evaluate the effects of the packet selection method to maintain the orthogonality to the excitation signal described in § 3.2. We deliberately chose the case with unbalanced numbers of coefficients 1 and -1. We change the unbalanced number from 0 (with our packet selection method) to 5. We set the source-to-AP distance equal to the tag-to-AP distance. The incident angle for the excitation signal is 0 degrees and the incident angle for the backscatter signal is 45 degrees. We measure the angle estimation as the unbalanced number increases. As shown in Fig. 19, when the number of coefficients 1 and -1 are equal, Willow outputs the target angle estimation with low error. However, because of the tremendous power differences between the excitation and backscatter signal, even if there is just one more coefficient 1, the leaked energy in the formed nonorthogonal pattern will greatly distort the estimated angle error to 11.5 degrees. When there are more than 2 extra coefficients 1, almost only the excitation signal can be shown in the MUSIC spectrum, so the output result is the AoA of the excitation signal, which has an error of approximately 45 degrees.

6.1.10 Tracking Objects. We move the tag across a U-shaped trajectory in an open field (6 m in length and 3 m in width). And we collect the location results by 4 APs at different points along this trajectory. We show the ground truth trajectory and corresponding inferred trajectory by Willow in Fig. 20. Because of the high localization accuracy, it allows us to faithfully capture the shape of the ground truth trajectory.

6.2 Parallel Localization

In this section, we examine the parallel localization performance. We first examine different impacting factors to parallel localization and then show the overall parallel localization performance in a real-deployed testbed.

6.2.1 Near-far problem. Willow uses various methods including orthogonal coefficient, iterative elimination, and location filtering to mitigate the near-far problem. However, TagFi calculates the location in the same MUSIC spectrum, in which the tag with a weaker signal strength will be greatly influenced by a stronger one. We experiment to evaluate the robustness of the near-far problem for both systems. We first assign two orthogonal coefficient patterns to tag#1 and tag#2. Then, we set the incident angle of the tag #1 and #2 to 20 degrees and 60 degrees. The distance between tag #2 and the AP is three times that of tag #1. We measure the angle estimation error for tag #2 with and without tag #1. We also connect tag #2 with 10 dB attenuation and test the error. We implement three versions of Willow. The first one uses synchronized tags, called Willow. The second one uses unsynchronized tags and with the iterative elimination and location filtering method, called Willow-I. The third one uses unsynchronized tags and without those methods, which is called Willow-II.

The result is shown in Fig. 21. When there's only tag #2 transmitting, it is marked as "1 Tag". Willow uses full orthogonal patterns, it reaches nearly the same AoA estimation error of around 5.4 degrees regardless of the presence of tag #1. Willow-I and Willow-II also achieve similar accuracy. But for TagFi, even with 1 tag, it exhibits a higher error of 10.4 degrees, due to the interference from the excitation signal. With 2 tags, the estimation error grows to be 14.4 degrees. To make matters worse, after connecting the attenuator, the errors for TagFi with 1 and 2 tags are 13.4 and 19.6 degrees respectively, as shown in Fig. 22. For Willow, it achieves a similar error of around 8.1 degrees with a single and two parallel tags. Because of the 10 dB attenuation, Willow-II is easier to be influenced by the interference from tag #1, increasing the error to 8.7 degrees. After applying our method, Willow-I achieves a similar error as the case with only 1 tag. The results show that Willow has better resistance to the near-far problem than the previous work.

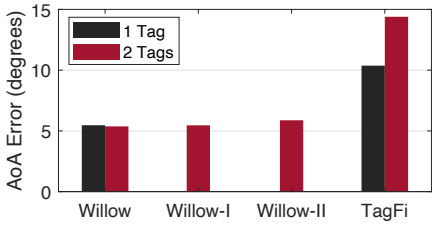

Figure 21: AoA error in placement 1 with 0 dB attenuation.

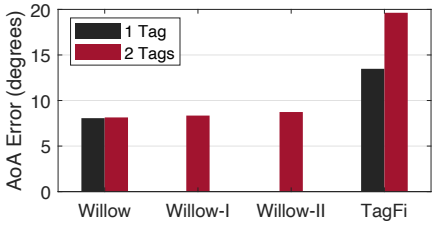

Figure 22: AoA error in placement 1 with 10 dB attenuation.

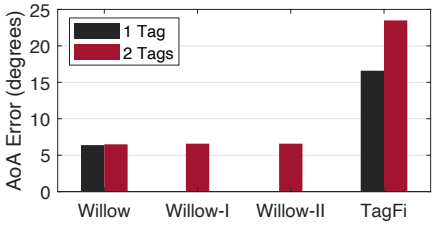

Figure 23: AoA error in placement 2 with 0 dB attenuation.

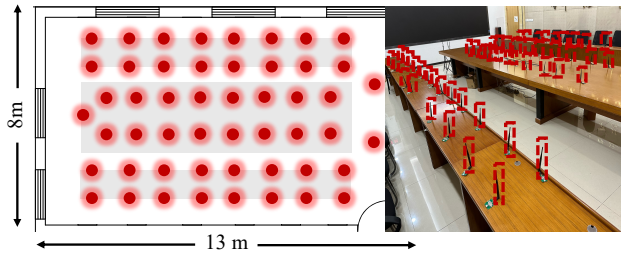

Figure 24: Placement of 51 parallel tags.

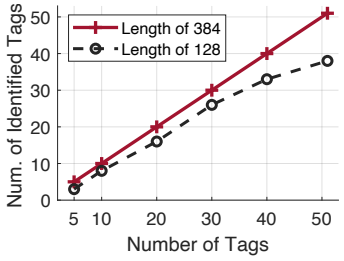

Figure 25: Detected tag amount.

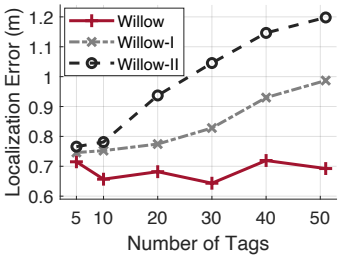

Figure 26: Mean error.

6.2.2 Impact of the geometrical relationship between tags. We then change the geometrical relationship between tag #1 and #2 to evaluate its impact. We keep the incident angle for tag #1 to 20 degrees and set it for tag #2 to 30 degrees. Then we keep the distance between tag and AP the same for both tags. And we still measure the AoA error for tag #2 with and without tag #1. The result is shown in Fig. 23. Because of the same localization distance, there should be less interference to tag #2. Willow and Willow-I indeed achieve similar AoA estimation errors of around 6.5 degrees with and without tag #1 transmission. Willow-II increases the error to 6.8 degrees. However, for TagFi, the AoA estimation error is even larger when there's a stronger near-far problem. This is because TagFi calculates the AoA in the same MUSIC spectrum. When the geometrical relationship is closer for tags, there will be more interference between them. Willow is more robust for different deployment situations.

6.2.3 Deployment in the Field. Finally, we deploy 51 tags in a meeting room as shown in Fig. 24. The tags are assigned with different orthogonal patterns in advance. The excitation source and AP are all commodity WiFi NICs AX200.

Tag detection. We first test if Willow can detect different tags with the assigned coefficient pattern. We use a sliding window to correlate the received CSI sequence with the predefined backscatter coefficient pattern and check if the absolute exceeds the threshold value. Tag detection is the precondition of localization, and it can also meet tasks such as object recognition. We test how many tags can be detected with different pattern lengths. The result is shown in Fig. 25. With a pattern length of 384, Willow successfully detects every tag linearly. With a pattern length of 128, as the number of tags increases, Willow can detect more tags, but there is a greater number of misread tags. Eventually, Willow detects 38 tags out of 51 tags with 128 pattern length. The pattern length of 384 will cause bigger latency but provide a more robust tag detection function. Thus, we use this pattern length to localize every tag.

Localization accuracy. In this experiment, we start with only 5 tags and gradually increase the number of tags to 51. Every time there are a few more tags added to the network, we measure the mean localization error. We use 7 APs to capture the backscatter coefficient pattern. We also develop different versions of Willow, which are Willow, Willow-I, and Willow-II, the same as in § 6.2.1. The result is shown in Fig. 26. Theoretically, our method supports as many tags as possible if patterns are orthogonal to each other. With the full orthogonal patterns, Willow does achieve a similar localization error of around 69 cm regardless of the number of tags. However, the increase in unsynchronized tags will lead to higher errors. For Willow-II, its error grows rapidly with the number of tags. We find that even after there are only 10 tags, the localization error of Willow-II has a sudden increase. It's because there are two tags with a very strong signal strength that consistently interfere with others. Finally, it reaches a mean localization error of 119 cm when there are 51 tags. With the method of iterative elimination and location filtering, Willow-I greatly reduces the localization error for Willow-II. It finally reaches a mean error of 98 cm. However, TagFi can't provide parallel localization even for 5 tags. The maximum supported concurrent number is 3. Thus, Willow extends the localization network by 17× without a reduction in the accuracy.

7 RELATED WORKS

Backscatter communication. Research on WiFi backscatter technology has attracted widespread attention in recent years. Hitchhike [32] embeds data on ambient Wi-Fi packets by converting the excitation Wi-Fi codeword to another valid codeword. WiTAG [46] alters the wireless channel to communicate data by leveraging MAC-layer features. Wi-Fi Backscatter [47] transmits data bits by

changing the RSSI of Wi-Fi packets. BackFi [48] and Hitchhike [32] change the phase of the incoming Wi-Fi signal to transmit data bits. Interscatter [49] uses a single-tone signal sent by a BLE device as an excitation signal to generate a legitimate Wi-Fi signal. OFDMA Backscatter [50] and Digiscatter [51] enable OFDMA in Wi-Fi backscatter tags. P^2LoRa [24] designs a parallel backscatter for ambient LoRa signal. Prism [52] scales the LoRa backscatter networks with non-linear chirps. Some papers [53, 54] work on enabling CDMA for backscatter with single-tone excitation. We can't directly use the current CDMA method in WiFi networks. Because the constraint in WiFi packet format and uniform distribution of WiFi signal raises new challenges. Willow uses the specific pattern design and interference cancellation method to adapt to WiFi traffic. SD-PHY Backscatter [55] enables software-defined PHY for backscatter communication and can generate WiFi packets. Leggiero [35] uses extra spatial sounding features to embed data into special format WiFi packets. OFDMA downlink [56] transforms the digital demodulation approach into the filtering-based analog one. SyncScatter [57] achieves accurate synchronization with ambient WiFi signals and realizes the maximum possible sensitivity. MOXcatter [58] embeds the tag data on ambient spatial-stream packets. X-tandem [59] achieves multi-hop backscatter communication in WiFi networks. Freerider [60] frequency shifts and transfers the code of ambient WiFi packets. TiScatter [61] encodes backscatter data into the timespan between two WiFi codewords. Chameleon [62] demodulates ambient WiFi and generates arbitrary carriers into valid WiFi packets. Some papers work on compressive sensing methods to recover the data sent by parallel tags [54, 63, 64] for communication purposes. They distinguish the wireless channel by the possibility from one state to another. As the number of tags increases, the complexity of the algorithm grows exponentially. Unlike Willow tags, the bits they send are defined by the pattern in advance. So, we can obtain channel state by using the orthogonality among patterns. So Willow can provide more accurate and larger-scale backscatter localization.

Backscatter localization. To lower the power of tags, backscatter localization systems use a variety of information to locate backscatter tags. Tagoram [65] leverages the mobility of RFID tags to construct a virtual antenna array to achieve precise localization. RFind [4] and TurboTrack [14] compose a large bandwidth of the backscatter signal from the RFID tag to enable 3D localization. RF-IDraw [66] uses antennae with different spacing to achieve high-resolution RFID localization. TurboTrack [14] uses a pipelined architecture and a Bayesian spacetime super-resolution algorithm to provide fine-grained localization. Millimetro [17] designs a millimeter wave tag to achieve long-distance and high-precision localization. P2PLocate [67] utilizes the assistant from the backscatter tag to locate other WiFi devices. MetaSight [68] designs a metasurface to read the NLoS RFID tags. μlocate [1] combines signals from multiple ISM bands to achieve accurate ToF estimation of LoRa backscatter. LocRa [2] enables accurate LoRa backscatter localization with spatially dispersed base stations. To achieve more ubiquitous localization, recent studies utilize existing WiFi devices to locate backscatter tags. WiTag [6] frequency shifts the excitation signal and calculates the location of the tag in the new band. TagFi [7] adapts a MUSIC-based algorithm to locate WiFi backscatter tags. Batch Localization [8] assigns different subcarriers to different backscatter tags for parallel localization.

8 CONCLUSION

We propose Willow, the first WiFi backscatter localization system for large-scale parallel tags. We design a packet-level orthogonal backscatter modulation method to embed backscatter signals into ambient WiFi traffic. We show that backscatter signals can be effectively extracted even under strong in-band WiFi interference. To adapt to real WiFi traffic, we propose a packet selection method to retain the orthogonality between backscatter signals and the WiFi signal. For parallel localization with multiple tags, we eliminate the inter-tag interference by an iterative signal cancellation method. We remove the location ambiguity and improve localization accuracy by designing a location filtering approach. We prototype Willow tags using custom low-cost hardware and use commodity WiFi NICs (i.e., Intel AX200) as the excitation source and Willow AP. The evaluation results show that Willow achieves a median localization error of 27 cm and supports 51 parallel tags, which is 2× and 17× better than the state-of-the-art method.

9 ACKNOWLEDGMENTS

We thank the shepherd Professor Swarun Kumar and anonymous reviewers for their insightful comments to improve the quality of our work. This work is in part supported by National Key R&D Program of China 2022YFC3801300, National Natural Science Foundation of China (U22A2031, No. 61932013, 62172250). Jiliang Wang is the corresponding author.

REFERENCES

[1] Rajalakshmi Nandakumar, Vikram Iyer, and Shyamnath Gollakota. 3d localization for sub-centimeter sized devices. In *Proceedings of ACM Sensys*, 2018.
[2] Jinyan Jiang, Jiliang Wang, Yijie Chen, Yihao Liu, and Yunhao Liu. LocRa: Enable Practical Long-Range Backscatter Localization for Low-Cost Tags. In *Proceedings of ACM Mobisys*, 2023.
[3] Bo Liang, Purui Wang, Renjie Zhao, Heyu Guo, Pengyu Zhang, Junchen Guo, Shunmin Zhu, Hongqiang Harry Liu, Xinyu Zhang, and Chenren Xu. RF-Chord: Towards deployable RFID localization system for logistic networks. In *Proceedings of USENIX NSDI*, 2023.
[4] Yunfei Ma, Nicholas Selby, and Fadel Adib. Minding the billions: Ultra-wideband localization for deployed rfid tags. In *Proceedings of ACM MobiCom*, 2017.
[5] Marco Cominelli, Francesco Gringoli, and Renato Lo Cigno. Passive device-free multi-point csi localization and its obfuscation with randomized filtering. In *Proceedings of IEEE MedComNet*, 2021.
[6] Manikanta Kotaru, Pengyu Zhang, and Sachin Katti. Localizing low-power backscatter tags using commodity wifi. In *Proceedings of ACM CoNEXT*, 2017.
[7] Elahe Soltanaghaei, Adwait Dongare, Akarsh Prabhakara, Swarun Kumar, Anthony Rowe, and Kamin Whitehouse. Tagfi: Locating ultra-low power wifi tags using unmodified wifi infrastructure. In *Proceedings of ACM UbiComp*, 2021.
[8] Xinyu Tong, Fengyuan Zhu, Yang Wan, Xiaohua Tian, and Xinbing Wang. Batch localization based on ofdma backscatter. In *Proceedings of ACM UbiComp*, 2019.
[9] Jian-feng ZHU, Xin-sheng HE, and Ben-jian HAO. A hybrid localization technology for an aerial moving target based on tdoa of dual-satellite and doa of main satellite. *ACTA ELECTONICA SINICA*, 46(6):1378, 2018.
[10] Qin Shi, Sihao Zhao, Xiaowei Cui, Mingquan Lu, and Mengdi Jia. Anchor self-localization algorithm based on uwb ranging and inertial measurements. *Tsinghua Science and Technology*, 24(6):728–737, 2019.
[11] Chenren Xu, Kenuo Xu, Lilei Feng, and Bo Liang. Retrov2x: A new vehicle-to-everything (v2x) paradigm with visible light backscatter networking. *Fundamental Research*, 2023.
[12] Atul Bansal, Akshay Gadre, Vaibhav Singh, Anthony Rowe, Bob Iannucci, and Swarun Kumar. OwLL: Accurate LoRa Localization using the TV Whitespaces. In *Proceedings of ACM/IEEE IPSN*, 2021.
[13] Deepak Vasisht, Swarun Kumar, and Dina Katabi. Decimeter-Level localization with a single WiFi access point. In *Proceedings of USENIX NSDI*, 2016.

[14] Zhihong Luo, Qiping Zhang, Yunfei Ma, Manish Singh, and Fadel Adib. 3d backscatter localization for fine-grained robotics. In *Proceedings of USENIX NSDI*, 2019.

[15] Suraj Jog, Junfeng Guan, Sohrab Madani, Ruochen Lu, Songbin Gong, Deepak Vasisht, and Haitham Hassanieh. Enabling IoT Self-Localization Using Ambient 5G Signals. In *Proceedings of USENIX NSDI*, 2022.

[16] Alexander Canals, Pascal Josephy, Simon Tanner, and Roger Wattenhofer. Robust indoor localization with ADS-B. In *Proceedings of ACM Mobicom*, 2021.

[17] Elahe Soltanaghaei, Akarsh Prabhakara, Artur Balanuta, Matthew Anderson, Jan M Rabaey, Swarun Kumar, and Anthony Rowe. Millimetro: mmwave retro-reflective tags for accurate, long range localization. In *Proceedings of ACM MobiCom*, 2021.

[18] Ali Abedi and Deepak Vasisht. Non-cooperative wifi localization & its privacy implications. In *Proceedings of ACM MobiCom*, 2022.

[19] Alejandro Blanco Pizarro, Joan Palacios Beltrán, Marco Cominelli, Francesco Gringoli, and Joerg Widmer. Accurate ubiquitous localization with off-the-shelf ieee 802.11 ac devices. In *Proceedings of ACM Mobisys*, 2021.

[20] Alex T Mariakakis, Souvik Sen, Jeongkeun Lee, and Kyu-Han Kim. Sail: Single access point-based indoor localization. In *Proceedings of ACM Mobisys*, 2014.

[21] Zhihao Gu, Taiwei He, Junwei Yin, Yuedong Xu, and Jun Wu. Tyrloc: a low-cost multi-technology mimo localization system with a single rf chain. In *Proceedings of ACM MobiSys*, 2021.

[22] U.S. Space Force. GPS: The Global Positioning System. https://www.gps.gov/.

[23] Mehrdad Hessar, Ali Najafi, and Shyamnath Gollakota. Netscatter: Enabling large-scale backscatter networks. In *Proceedings of USENIX NSDI*, 2019.

[24] Jinyan Jiang, Zhenqiang Xu, Fan Dang, and Jiliang Wang. Long-range ambient LoRa backscatter with parallel decoding. In *Proceedings of ACM MobiCom*, 2021.

[25] Jie Xiong, Karthikeyan Sundaresan, and Kyle Jamieson. Tonetrack: Leveraging frequency-agile radios for time-based indoor wireless localization. In *Proceedings of ACM MobiCom*, 2015.

[26] Jie Xiong and Kyle Jamieson. Arraytrack: A fine-grained indoor location system. In *Proceedings of USENIX NSDI*, 2013.

[27] Elahe Soltanaghaei, Avinash Kalyanaraman, and Kamin Whitehouse. Multipath Triangulation: Decimeter-Level WiFi Localization and Orientation with a Single Unaided Receiver. In *Proceedings of ACM MobiSys*, 2018.

[28] Manikanta Kotaru, Kiran Joshi, Dinesh Bharadia, and Sachin Katti. Spotfi: Decimeter level localization using wifi. In *Proceedings of ACM SIGCOMM*, 2015.

[29] MC Vanderveen, BC Ng, CB Papadias, and A Paulraj. Joint angle and delay estimation (jade) for signals in multipath environments. In *Proceedings of IEEE Asilomar Conference on Signals, Systems and Computers*, 1996.

[30] Tianjian Ji and Aikaterini Pachi. Frequency and velocity of people walking. *Struct. Eng*, 84(3):36–40, 2005.

[31] Wiki. Central limit theorem — Wikipedia, the free encyclopedia. http://en.wikipedia.org/w/index.php?title=Central%20limit%20theorem&oldid=1181876776.

[32] Pengyu Zhang, Dinesh Bharadia, Kiran Joshi, and Sachin Katti. Hitchhike: Practical backscatter using commodity WiFi. In *Proceedings of ACM Sensys*, 2016.

[33] Timo Pfau, Sebastian Hoffmann, and Reinhold Noé. Hardware-efficient coherent digital receiver concept with feedforward carrier recovery for m-qam constellations. *Journal of Lightwave Technology*, 27(8):989–999, 2009.

[34] Dae Gil Yoon, Soo Young Shin, Wook Hyun Kwon, and Hong Seong Park. Packet error rate analysis of ieee 802.11 b under ieee 802.15. 4 interference. In *Proceedings of IEEE VTC*, 2006.

[35] Xin Na, Xiuzhen Guo, Zihao Yu, Jia Zhang, Yuan He, and Yunhao Liu. Leggiero: Analog wifi backscatter with payload transparency. In *Proceedings of ACM MobiSys*, 2023.

[36] Shuai Tong, Jiliang Wang, and Yunhao Liu. Combating packet collisions using non-stationary signal scaling in LPWANs. In *Proceedings of ACM MobiSys*, 2020.

[37] Shyamnath Gollakota and Dina Katabi. Zigzag decoding: Combating hidden terminals in wireless networks. In *Proceedings of ACM SIGCOMM*, 2008.

[38] Mohamad Katanbaf, Anthony Weinand, and Vamsi Talla. Simplifying backscatter deployment:{Full-Duplex}{LoRa} backscatter. In *Proceedings of USENIX NSDI*, 2021.

[39] Analog Devices. ADG902. https://www.analog.com/media/en/technical-documentation/data-sheets/ADG901_902.pdf.

[40] STMicroelectronics. STM32L011D3P6. https://www.st.com/resource/en/datasheet/stm32l011d4.pdf.

[41] Skyworks. SKY7630-005LF: Surface-mount mixer and detector schottky diodes.

[42] Texas Instruments. LPV7215MG. https://www.ti.com/store/ti/en/p/product/?p=LPV7215MG/NOPB.

[43] Intel. AX200 WiFi NICs. https://www.intel.sg/content/www/xa/en/products/sku/204836/intel-wifi-6e-ax210-gig/specifications.html.

[44] Zhiping Jiang, Tom H. Luan, Xincheng Ren, Dongtao Lv, Han Hao, Jing Wang, Kun Zhao, Wei Xi, Yueshen Xu, and Rui Li. Eliminating the Barriers: Demystifying Wi-Fi Baseband Design and Introducing the PicoScenes Wi-Fi Sensing Platform. *IEEE Internet of Things Journal*, 9(6):4476–4496, 2022.

[45] Zhiping Jiang. PicoScenes. https://ps.zpj.io/hardware.html.

[46] Ali Abedi, Farzan Dehbashi, Mohammad Hossein Mazaheri, Omid Abari, and Tim Brecht. Witag: Seamless wifi backscatter communication. In *Proceedings of ACM SIGCOMM*, 2020.

[47] Bryce Kellogg, Aaron Parks, Shyamnath Gollakota, Joshua R Smith, and David Wetherall. WiFi backscatter: Internet connectivity for RF-powered devices. In *Proceedings of ACM SIGCOMM*, 2014.

[48] Dinesh Bharadia, Kiran Raj Joshi, Manikanta Kotaru, and Sachin Katti. Backfi: High throughput wifi backscatter. In *Proceedings of ACM SIGCOMM*, 2015.

[49] Vikram Iyer, Vamsi Talla, Bryce Kellogg, Shyamnath Gollakota, and Joshua Smith. Inter-technology backscatter: Towards internet connectivity for implanted devices. In *Proceedings of ACM SIGCOMM*, 2016.

[50] Renjie Zhao, Fengyuan Zhu, Yuda Feng, Siyuan Peng, Xiaohua Tian, Hui Yu, and Xinbing Wang. OFDMA-enabled WiFi backscatter. In *Proceedings of ACM MobiCom*, 2019.

[51] Fengyuan Zhu, Yuda Feng, Qianru Li, Xiaohua Tian, and Xinbing Wang. DigiScatter: efficiently prototyping large-scale OFDMA backscatter networks. In *Proceedings of ACM MobiSys*, 2020.

[52] Yidong Ren, Puyu Cai, Jinyan Jiang, Jialuo Du, and Zhichao Cao. Prism: High-throughput lora backscatter with non-linear chirps. In *Proceedings of IEEE INFOCOM*, 2023.

[53] Nanhuan Mi, Xiaoxue Zhang, Xin He, Jie Xiong, Mingjun Xiao, Xiang-Yang Li, and Panlong Yang. Cbma: Coded-backscatter multiple access. In *Proceedings of IEEE ICDCS*, 2019.

[54] Jue Wang, Haitham Hassanieh, Dina Katabi, and Piotr Indyk. Efficient and reliable low-power backscatter networks. *ACM SIGCOMM Computer Communication Review*, 42(4):61–72, 2012.

[55] Fengyuan Zhu, Mingwei Ouyang, Luwei Feng, Yaoyu Liu, Xiaohua Tian, Meng Jin, Dongyao Chen, and Xinbing Wang. Enabling software-defined phy for backscatter networks. In *Proceedings of ACM MobiSys*, 2022.

[56] Fengyuan Zhu, Luwei Feng, Meng Jin, Xiaohua Tian, Xinbing Wang, and Chenghu Zhou. Towards ultra-low power ofdma downlink demodulation. In *Proceedings of ACM Sensys*, 2022.

[57] Manideep Dunna, Miao Meng, Po-Han Wang, Chi Zhang, Patrick Mercier, and Dinesh Bharadia. SyncScatter: Enabling WiFi like synchronization and range for WiFi backscatter Communication. In *Proceedings of USENIX NSDI*, 2021.

[58] Jia Zhao, Wei Gong, and Jiangchuan Liu. Spatial stream backscatter using commodity wifi. In *Proceedings of ACM MobiSys*, 2018.

[59] Jia Zhao, Wei Gong, and Jiangchuan Liu. X-tandem: Towards multi-hop backscatter communication with commodity wifi. In *Proceedings of ACM Mobicom*, 2018.

[60] Pengyu Zhang, Colleen Josephson, Dinesh Bharadia, and Sachin Katti. Freerider: Backscatter communication using commodity radios. In *Proceedings of ACM CoNEXT*, 2017.

[61] Caihui Du, Jiahao Liu, Shuai Wang, Rongrong Zhang, Wei Gong, and Jihong Yu. Timespan-based backscatter using a single cots receiver. In *Proceedings of ACM MobiSys*, 2023.

[62] Longzhi Yuan and Wei Gong. Enabling native wifi connectivity for ambient backscatter. In *Proceedings of ACM MobiSys*, 2023.

[63] Meng Jin, Yuan He, Xin Meng, Yilun Zheng, Dingyi Fang, and Xiaojiang Chen. Fliptracer: Practical parallel decoding for backscatter communication. In *Proceedings of ACM MobiCom*, 2017.

[64] Pan Hu, Pengyu Zhang, and Deepak Ganesan. Laissez-faire: Fully asymmetric backscatter communication. *ACM SIGCOMM computer communication review*, 45(4):255–267, 2015.

[65] Lei Yang, Yekui Chen, Xiang-Yang Li, Chaowei Xiao, Mo Li, and Yunhao Liu. Tagoram: real-time tracking of mobile RFID tags to high precision using COTS devices. In *Proceedings of ACM MobiCom*, 2014.

[66] Jue Wang, Deepak Vasisht, and Dina Katabi. RF-IDraw: virtual touch screen in the air using RF signals. In *Proceedings of ACM SIGCOMM*, 2014.

[67] Xianan Zhang, Wei Wang, Xuedou Xiao, Hang Yang, Xinyu Zhang, and Tao Jiang. Peer-to-peer localization for single-antenna devices. In *Proceedings of ACM UbiComp*, 2020.

[68] Dianhan Xie, Xudong Wang, and Aimin Tang. Metasight: Localizing blocked rfid objects by modulating nlos signals via metasurfaces. In *Proceedings of ACM MobiSys*, 2022.